PHYSICAL REVIEW B **73**, 014113 (2006)

Three intrinsic relationships of lattice parameters between intermediate monoclinic M_C and tetragonal phases in ferroelectric $Pb[(Mg_{1/3}Nb_{2/3})_{1-x}Ti_x]O_3$ and $Pb[(Zn_{1/3}Nb_{2/3})_{1-x}Ti_x]O_3$ near morphotropic phase boundaries

Yu U. Wang*
Department of Materials Science and Engineering, Virginia Tech, Blacksburg, Virginia 24061, USA
(Received 17 September 2005; published 25 January 2006)

Systematic analysis of extensive experimental data confirms the theoretical prediction of three intrinsic relationships of lattice parameters between the recently discovered intermediate monoclinic M_C phase and the conventional tetragonal phase in ferroelectric $Pb[(Mg_{1/3}Nb_{2/3})_{1-x}Ti_x]O_3$ and $Pb[(Zn_{1/3}Nb_{2/3})_{1-x}Ti_x]O_3$ near the morphotropic phase boundaries. These intrinsic relationships of lattice parameters are fulfilled by experimental data reported in the literature for different temperatures, compositions, and electric fields. They present quantitative evidence that the intermediate monoclinic M_C phase is a mixed state of nanometer-sized twin-related domains of the conventional ferroelectric tetragonal phase. The analysis supports the concept recently proposed by Khachaturyan and co-workers [Phys. Rev. Lett. **91**, 197601 (2003)] that the intermediate monoclinic M_C phase is adaptive ferroelectric and ferroelastic phase, which is homogeneous only on the macroscale while inhomogeneous on the nanoscale. Due to the small domain size and small ferroelastic strain, the conventional diffraction measurement does not resolve the lattice of individual nanodomains rather instead only perceives the average diffraction effect of nanotwins, yielding the experimentally observed monoclinic symmetry. The result indicates that the electric-field-induced domain-wall movement plays an essential role in the ultrahigh electromechanical responses of $Pb[(Mg_{1/3}Nb_{2/3})_{1-x}Ti_x]O_3$ and $Pb[(Zn_{1/3}Nb_{2/3})_{1-x}Ti_x]O_3$, and the high-density domain walls associated with the nanotwins have a significant contribution to the peculiar material properties near the morphotropic phase boundaries.

DOI: 10.1103/PhysRevB.73.014113 PACS number(s): 77.84.−s, 77.65.−j

I. INTRODUCTION

Multiferroics are smart, active, and multifunctional materials with domain microstructures that actively respond to changes in external mechanical, electric, magnetic, and thermal conditions. They form the basis for a wide variety of sensors, actuators, and microdevices. As an important category of multiferroics, ferroelectric-ferroelastic perovskites $Pb[(Mg_{1/3}Nb_{2/3})_{1-x}Ti_x]O_3$ (PMN-*x*PT) (Ref. 1) and $Pb[(Zn_{1/3}Nb_{2/3})_{1-x}Ti_x]O_3$ (PZN-*x*PT) (Ref. 2) are currently under intensive investigation for both technological importance and scientific curiosity. Single crystals of the relaxor-based ferroelectric PMN-*x*PT and PZN-*x*PT with compositions near their respective morphotropic phase boundaries (MPBs) exhibit ultrahigh piezoelectric responses an order of magnitude greater than that of the conventional polycrystalline $Pb(Zr_{1-x}Ti_x)O_3$ (PZT) ceramics,[3] which is currently the material of choice for a wide variety of high-performance electromechanical sensors and actuators.[4–6] PMN-*x*PT and PZN-*x*PT promise to revolutionize the world of piezoelectric and electrostrictive devices.[7]

PMN-*x*PT and PZN-*x*PT have qualitatively similar temperature-composition phase diagrams: The high-temperature paraelectric phases have a cubic perovskite structure, and the low-temperature ferroelectric phases have a rhombohedral symmetry at low PT content and a tetragonal symmetry at high PT content. The MPB is the boundary of an abrupt structural change between the two forms,[4] i.e., rhombohedral and tetragonal. Recent extensive experimental investigations have discovered new intermediate phases and revealed fascinating while puzzling phase behaviors around the MPBs.[8–22]

Since the recent discovery of an intermediate monoclinic M_A phase in PZT near its MPB,[23–28] new intermediate phases have also been discovered in PZN-*x*PT and PMN-*x*PT near their respective MPBs, namely, monoclinic M_A,[8–10] monoclinic M_C,[8–12] orthorhombic (Refs. 8 and 13–15) phases in PZN-*x*PT, and orthorhombic,[16,17] monoclinic M_C,[12,18–21] monoclinic M_A,[21,22] as well as a third monoclinic M_B phase (Refs. 17 and 20) in PMN-*x*PT, depending on thermal and electric histories. Structural phase transformations have been revealed in PZN-*x*PT (Refs. 8–10) and PMN-*x*PT (Refs. 17 and 21) under the effects of temperature and electric field. Unusual continuous polarization rotation in symmetry planes of the intermediate monoclinic phases is observed.[8–10,17,21]

The ultrahigh piezoelectric responses of PZN-*x*PT and PMN-*x*PT single crystals are related to the existence of MPBs, the newly discovered intermediate MPB phases, and the temperature- and electric field-dependent behaviors of these phases. The recently established temperature-composition phase diagrams[15,19] and electric-field-temperature phase diagrams[10,21] reveal some fundamental aspects of the phase stabilities in the vicinity of MPBs. The large body of reported experimental data[8–22] provides information to investigate the relations between the phases and to clarify the origin of the ultrahigh electromechanical properties of these materials.

Khachaturyan and co-workers[29–31] recently proposed an adaptive ferroelectric phase theory to explain the behaviors of intermediate monoclinic phases in PMN-*x*PT and PZN-*x*PT. According to this theory, the monoclinic phase is a mixed state of miniaturized domains of the conventional ferroelectric phase, which is inhomogeneous on the nanos-

cale while homogeneous on the macroscale. A change in the nanodomain morphology—caused by changes in external electric field, applied stress, temperature, or composition—results in a gradual adjustment of the nanodomain-averaged properties, e.g., lattice parameters, symmetry, spontaneous strain, and polarization. Two intrinsic relationships of lattice parameters (called invariance conditions) are predicted for the intermediate monoclinic M_C phase and examined against the experimental data reported in Ref. 16 in previous work.[29,30] In this work, we predict a third intrinsic relationship of lattice parameters concerning the monoclinic angle of the M_C phase.

The purpose of this paper is to present quantitative evidence for three intrinsic relationships between the lattice parameters (a_m, b_m, c_m, β) of the intermediate monoclinic M_C phases and the lattice parameters (a_t, c_t) of the conventional ferroelectric tetragonal phases in PMN-xPT and PZN-xPT. Systematic analysis shows that the three intrinsic relationships of lattice parameters are fulfilled by extensive experimental data of monoclinic M_C and tetragonal phases reported in the literature[9,10,14,15,19–21] for different temperatures, compositions, and electric fields. The analysis of the M_A and M_B phases will be reported elsewhere. The result indicates that the intermediate monoclinic M_C phase is a mixed state of tetragonal nanotwins. Experimental observations, e.g., anisotropic broadening of diffraction peak profiles, phase coexistence over wide temperature and composition ranges, and large electric-field-induced strain, are discussed in light of nanoscale twin microstructures. The effects of high-density domain walls associated with the nanotwins on the peculiar material properties near the morphotropic phase boundaries are also discussed.

II. CRYSTALLOGRAPHIC ANALYSIS

A homogeneous ferroelectric and ferroelastic state is unstable with respect to the formation of ferroelectric and ferroelastic domains.[32–34] The ferroelastic microstructure consists of several crystallographically equivalent structural domains with different orientations (called variants), e.g., three tetragonal variants. The variants self-assemble to form polydomain plates with domains arranged in twin-related patterns.[33,35–41] The relative thicknesses of the twin layers, specified by the volume fraction ω, self-adjust to establish macroscopic invariance of the habit plane (i.e., the macroscopic size of the habit plane is not affected by the ferroelastic transformation), and by doing so self-accommodate the spontaneous ferroelastic strain, eliminating the long-range stress field and minimizing the elastic energy.[33,35–41] The presence of ferroelectric polarization in the ferroelastic structural domains results in a formation of head-to-tail patterns of ferroelectric domains, which does not generate spatial charges and automatically minimizes the electrostatic energy. The volume fraction ω of the twin variants can be changed by external electric field and applied stress through domain-wall movement, leading to a macroscopic strain of the sample, which is of the same order of magnitude as the spontaneous strain of the ferroelastic variant.

The size of the domains is determined by the minimization of a sum of the domain-wall energy, elastic energy, and electrostatic energy.[29,30,33,42] For very low value of domain-wall energy density, the system transforms into a mixed state of miniaturized domains, which is inhomogeneous on the nanoscale while homogeneous on the macroscale.[29,30,42] A change in the nanodomain morphology—caused by changes in external electric field, applied stress, temperature, or composition—results in a gradual adjustment of the nanodomain-averaged properties, e.g., lattice parameters, symmetry, spontaneous strain, and polarization. Khachaturyan *et al.*[42] developed an adaptive phase theory to explain the experimental observation of self-adjusting intermediate ferroelastic (martensitic) states with variable crystal lattice parameters depending on temperature and applied stress in martensitic crystals.[43] This concept has recently been further developed to explain the behaviors of intermediate monoclinic phases in ferroelectric PMN-xPT and PZN-xPT.[29–31]

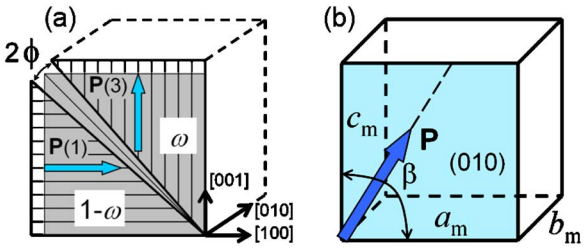

FIG. 1. (Color online) (a) Twin-related tetragonal variants with (101) twin plane, where the hatching direction indicates tetragonal axis orientation, and the gray shadow illustrates the crystal before ferroelastic transformation. The volume fractions of variants 1 and 3 are 1-ω and ω, respectively. The polarization in each structural variant is along the tetragonal axis. The averaged polarization is confined to and rotate in (010) symmetry plane. The averaged lattice has a monoclinic M_C symmetry. Closing the gap between the twin-related tetragonal variants caused by spontaneous ferroelastic strain gives rise to the monoclinic angle of the averaged lattice. (b) The monoclinic M_C unit cell resulting from averaging twin-related tetragonal variants shown in (a). Note that average is in a sense of a diffraction measurement that does not resolve the lattice of individual domains, but instead perceives only the average diffraction effect of nanotwins due to small domain size and small ferroelastic strain.

It has been shown that averaging the twin-related tetragonal nanodomains gives rise to the monoclinic M_C lattice symmetry, with monoclinic lattice parameters a_m, b_m, and c_m uniquely related to the tetragonal lattice parameters a_t and c_t.[29,30] We will show here that the monoclinic angle β is also determined by the tetragonal lattice parameters a_t and c_t. Thus, three intrinsic relationships are predicted between the lattice parameters of the intermediate monoclinic M_C and conventional tetragonal phases. It is noted that "average" is in a sense of diffraction measurement that does not resolve the lattice of individual domains but instead perceives only the average diffraction effect of nanotwins due to small domain size and small ferroelastic strain.

For the orientations of two twin-related tetragonal variants specified in Fig. 1(a), the nanodomain-averaged lattice has a monoclinic M_C symmetry shown in Fig. 1(b). The M_C lattice parameters are:[29,30]

$$a_m = a_t\omega + c_t(1-\omega) = c_t - (c_t - a_t)\omega, \tag{1}$$

$$c_m = c_t\omega + a_t(1-\omega) = a_t + (c_t - a_t)\omega, \tag{2}$$

$$b_m = a_t. \tag{3}$$

The monoclinic angle β of the averaged M_C lattice arises from the conservation of lattice continuity in a coherent microstructure, which is achieved through relative rigid-body rotation of the twin-related tetragonal variants to close the gap between them. The gap angle 2ϕ is caused by the spontaneous ferroelastic strain of the two twin-related tetragonal variants, as illustrated in Fig. 1(a). We postulate the monoclinic angle of the nanodomain-averaged lattice as:

$$\beta = \frac{\pi}{2} + 2A\omega(1-\omega)\phi, \tag{4}$$

where the angle ϕ is related to the tetragonality c_t/a_t of the tetragonal lattice:

$$\phi = \tan^{-1}\frac{c_t}{a_t} - \frac{\pi}{4}. \tag{5}$$

The dependence of β on the volume fraction ω is a simple quadratic function, which does not produce monoclinic lattice in the case of single tetragonal domains, i.e., $\omega=0$ or 1. The volume fraction can be determined from the measured monoclinic M_C lattice parameters by solving Eqs. (1)–(3) for ω:

$$\omega = \frac{c_m - b_m}{a_m + c_m - 2b_m}. \tag{6}$$

The coefficient A collects the effect of domain sizes on the experimental measurement of monoclinic angle by diffraction and scattering techniques, and is approximated as a constant of order of magnitude of 1.

Combining Eqs. (1) and (2) gives the *first intrinsic relationship* of lattice parameters between the intermediate monoclinic M_C phase and conventional tetragonal phase:

$$a_m + c_m = a_t + c_t. \tag{7a}$$

The *second intrinsic relationship* of lattice parameters is expressed by Eq. (3) and is renumbered in the following for convenience:

$$b_m = a_t. \tag{7b}$$

The *third intrinsic relationship* of lattice parameters is given by combining Eqs. (4) and (5):

$$\beta = \frac{\pi}{2} + 2A\omega(1-\omega)\left(\tan^{-1}\frac{c_t}{a_t} - \frac{\pi}{4}\right), \tag{7c}$$

where ω is determined by Eq. (6). In the range of monoclinic M_C phase, the values of tetragonal lattice parameters are determined from the measured monoclinic M_C lattice parameters by using Eqs. (7a) and (7b): $a_t=b_m$, $c_t=a_m+c_m-b_m$. The first two intrinsic relationships (7a) and (7b) are also called general invariance conditions.[29,30] It is worth noting that the second intrinsic relationship (7b), i.e., continuity between b_m and a_t, has been well recognized as a prominent feature in the reported experimental data[9,10,14,15,19–21] due to direct visual effect in data plots but without explanation.

The polarization in each structural variant is along the tetragonal axis, i.e., $\mathbf{P}(1)=(P_t,0,0)$ and $\mathbf{P}(3)=(0,0,P_t)$, where P_t is the magnitude of polarization in tetragonal phase. The polarization averaged over the twin-related variants is:[29,30]

$$\mathbf{P} = \mathbf{P}(3)\omega + \mathbf{P}(1)(1-\omega) = P_t(1-\omega,0,\omega), \tag{8}$$

which is confined to the symmetry plane (010) as illustrated in Fig. 1(b). When the volume fraction ω of the twin variants is changed by external electric field or applied stress through domain-wall movement, the averaged polarization $\mathbf{P}$ rotates in (010) plane, as experimentally observed in monoclinic M_C phase.

III. ANALYSIS OF EXPERIMENTAL DATA

The three intrinsic relationships of lattice parameters, Eqs. (7a)–(7c), can be directly examined by the experimental data of monoclinic M_C and tetragonal phases of PMN-xPT and PZN-xPT reported in the literature for different temperatures, compositions, and electric fields.[9,10,14,15,19–21] In this section, a systematic analysis of extensive experimental data is presented to show the fulfillment of the three intrinsic relationships of lattice parameters.

A. PMN-xPT

1. Temperature-dependent lattice parameters in zero-field cooling

a. PMN-31%PT. Noheda *et al.*[19] reported the temperature-dependent lattice parameters of PMN-31%PT in zero-field cooling by x-ray powder diffraction measurement as shown in Fig. 2(a). The first and second intrinsic relationships, Eqs. (7a) and (7b), are examined against the experimental data and highlighted by gray shadow in Fig. 2(b), where the first relationship is plotted with both sides of Eq. (7a) divided by 2 for visual clarity. The third intrinsic relationship, Eq. (7c), is examined in Fig. 2(c), where the monoclinic angle β is calculated according to Eq. (7c) with $A=1.45$ as a fitting parameter. In the M_C phase field, the volume fraction ω determined from the measured monoclinic lattice parameters, according to Eq. (6), is 0.570, 0.635, and 0.577 in cooling sequence. It is noted that at 350 K (approaching the M_C-tetragonal transition temperature), the experimentally measured a_m and c_m are so close to one another that they cannot be accurately determined, as indicated by the error bars in Fig. 2(a).

b. PMN-33%PT. Noheda *et al.*[19] reported the temperature-dependent lattice parameters of PMN-33%PT in zero-field cooling by x-ray powder diffraction measurement as shown in Fig. 3(a). The three intrinsic relationships are shown in Figs. 3(b) and 3(c), with $A=1.46$. In the M_C phase field, the determined volume fraction ω is 0.655 and 0.654 in cooling sequence.

c. PMN-37%PT. Noheda *et al.*[19] reported the temperature-dependent lattice parameters of PMN-37%PT in zero-field cooling by x-ray powder diffraction measurement as shown in Fig. 4(a). The three intrinsic relationships are

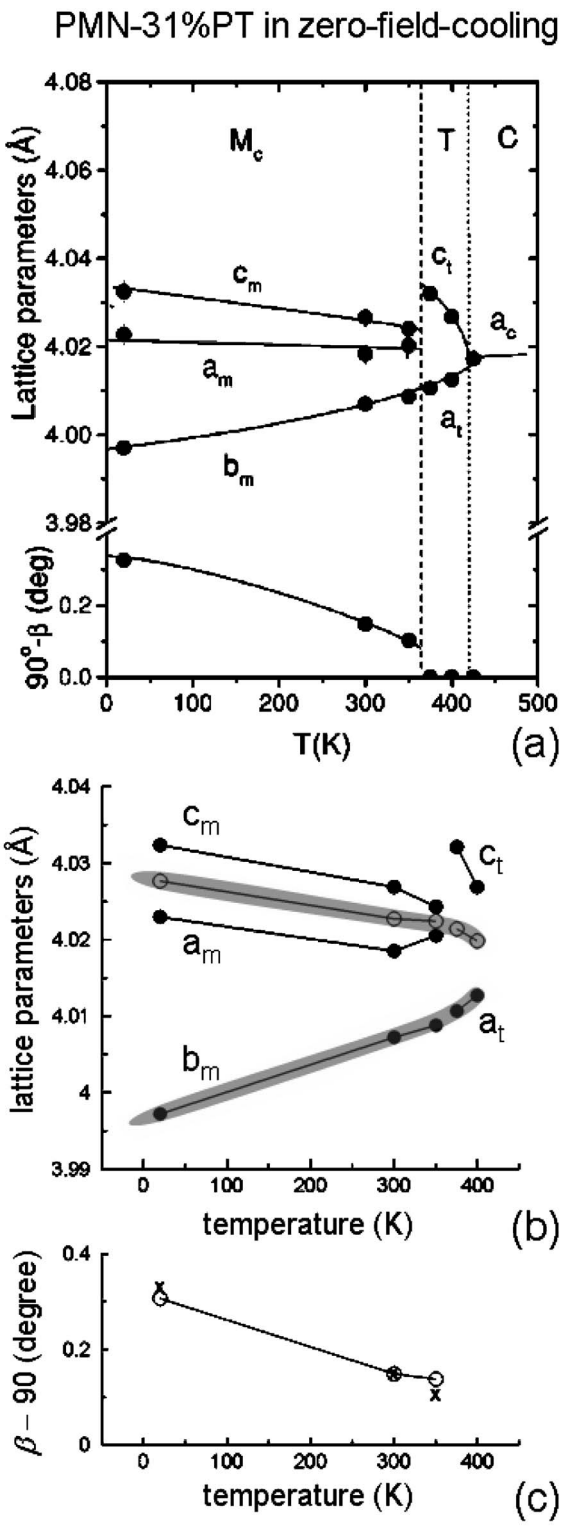

FIG. 2. Three intrinsic relationships of lattice parameters between the intermediate monoclinic M_C phase and conventional tetragonal phase of PMN-31%PT in zero-field cooling. (a) X-ray powder diffraction measurement of lattice parameters (reproduced with permission—Ref. 19). (b) The first and second intrinsic relationships are highlighted by gray shadow, where data are taken from (a). (c) The third intrinsic relationship is highlighted by line, where data of crosses (×) are taken from (a) and data of open circles (○) are calculated from Eq. (7c).

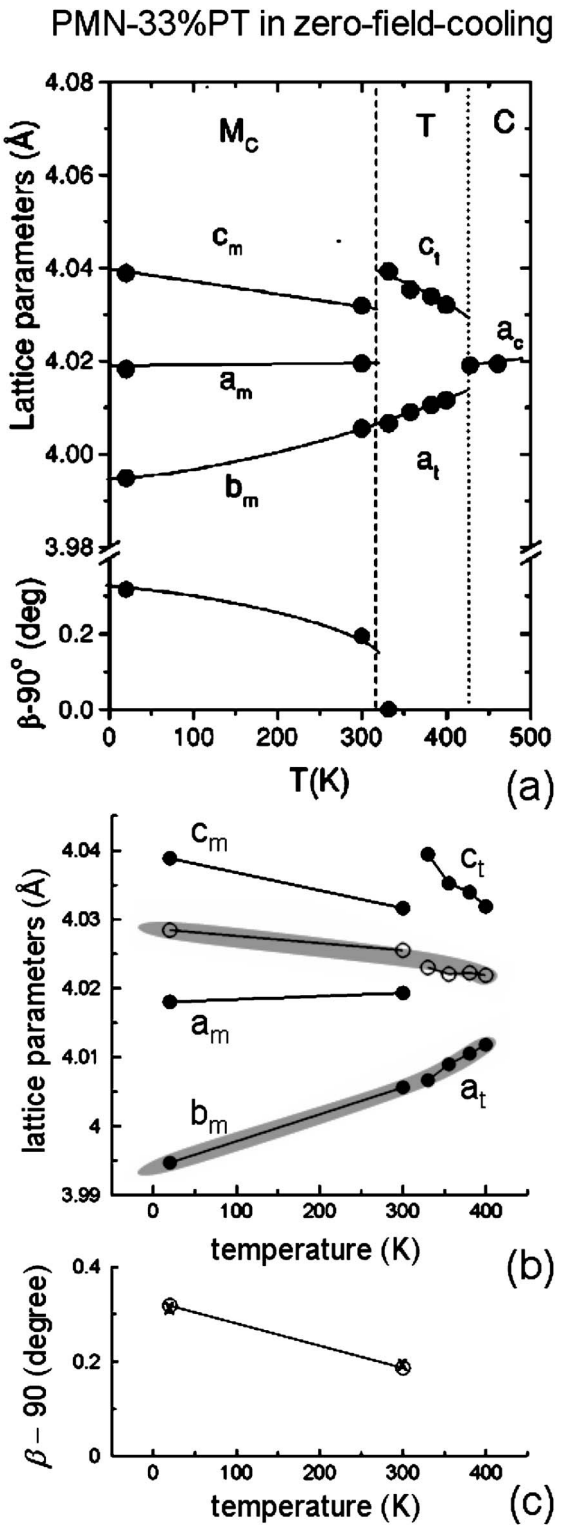

FIG. 3. Three intrinsic relationships of lattice parameters between the intermediate monoclinic M_C phase and conventional tetragonal phase of PMN-33%PT in zero-field cooling. (a) X-ray powder diffraction measurement of lattice parameters (reproduced with permission—Ref. 19). (b) The first and second intrinsic relationships are highlighted by gray shadow, where data are taken from (a). (c) The third intrinsic relationship is highlighted by line, where data of crosses (×) are taken from (a) and data of open circles (○) are calculated from Eq. (7c).

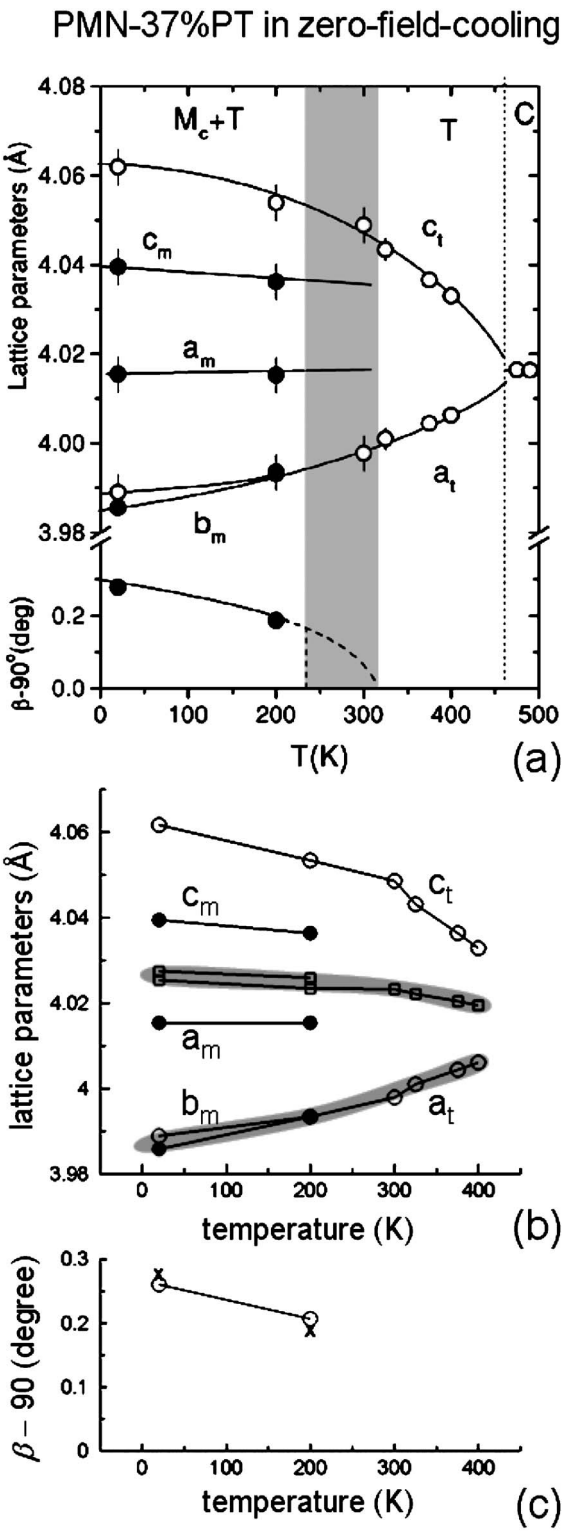

FIG. 4. Three intrinsic relationships of lattice parameters between the intermediate monoclinic M_C phase and conventional tetragonal phase of PMN-37%PT in zero-field cooling. (a) X-ray powder diffraction measurement of lattice parameters (reproduced with permission—Ref. 19). (b) The first and second intrinsic relationships are highlighted by gray shadow, where data are taken from (a). (c) The third intrinsic relationship is highlighted by line, where data of crosses (×) are taken from (a) and data of open circles (○) are calculated from Eq. (7c).

shown in Figs. 4(b) and 4(c), with $A=1.04$. In the M_C phase field, the determined volume fraction ω is 0.634 and 0.594 in cooling sequence. It is noted that the reported coexistence of monoclinic M_C and tetragonal phases over a wide temperature range between 20 K and 200 K allows a direct examination of the first and second intrinsic relationships over this temperature range in this case.

2. Composition-dependent lattice parameters in zero field

a. PMN-*x*PT *at* 300 K. Noheda *et al.*[19] reported the composition-dependent lattice parameters of PMN-*x*PT at 300 K by x-ray powder diffraction measurement as shown in Fig. 5(a). The three intrinsic relationships are shown in Figs. 5(b) and 5(c), with $A=1.51$. In the M_C phase field, the determined volume fraction ω is 0.634, 0.661, and 0.693 in increasing x sequence. It is noted that the reported data for composition $x=34\%$ are taken from a different experiment.

b. PMN-*x*PT *at* 20 K. Noheda *et al.*[19] reported the composition-dependent lattice parameters of PMN-*x*PT at 20 K by x-ray powder diffraction measurement as shown in Fig. 6(a). The three intrinsic relationships are shown in Figs. 6(b) and 6(c), with $A=1.45$. In the M_C phase field, the determined volume fraction ω is 0.594, 0.649, 0.745, and 0.642 in increasing x sequence. It is noted that the experimental error increases while approaching the M_C-tetragonal transition temperature, as indicated by the error bars in Fig. 6(a).

c. PMN-*x*PT *at room temperature*. Singh and Pandey[20] reported the composition-dependent lattice parameters of PMN-*x*PT at room temperature by x-ray powder diffraction measurement shown in Fig. 7(a), where the space groups Pm and P4mm correspond to monoclinic M_C and tetragonal phases, respectively. The three intrinsic relationships are shown in Figs. 7(b) and 7(c), with $A=1.20$. In the M_C phase field, the determined volume fraction ω is 0.612, 0.619, 0.608, and 0.630 in increasing x sequence.

3. Temperature-dependent lattice parameters in field cooling

Bai *et al.*[21] reported the temperature-dependent lattice parameters of PMN-30%PT in field cooling with a [001] electric field of 1 kV/cm by single crystal x-ray diffraction measurement as shown in Fig. 8(a). The three intrinsic relationships are shown in Figs. 8(b) and 8(c), with $A=0.74$. In the M_C phase field, the determined volume fraction ω is 0.610, 0.565, 0.557, and 0.550 in cooling sequence.

B. PZN-*x*PT

1. Composition-dependent lattice parameters in zero field

La-Orauttapong *et al.*[15] reported the composition-dependent lattice parameters of PZN-*x*PT at 20 K by x-ray powder diffraction measurement as shown in Fig. 9(a). The three intrinsic relationships are shown in Figs. 9(b) and 9(c), with $A=0.64$. It is noted that with the special value of volume fraction $\omega=\frac{1}{2}$, Eqs. (1) and (2) give $a_m=c_m$, and the monoclinic M_C symmetry is increased to orthorhombic symmetry, i.e., orthorhombic phase can be regarded as M_C phase in the limit of $a_m=c_m$.[8,14]

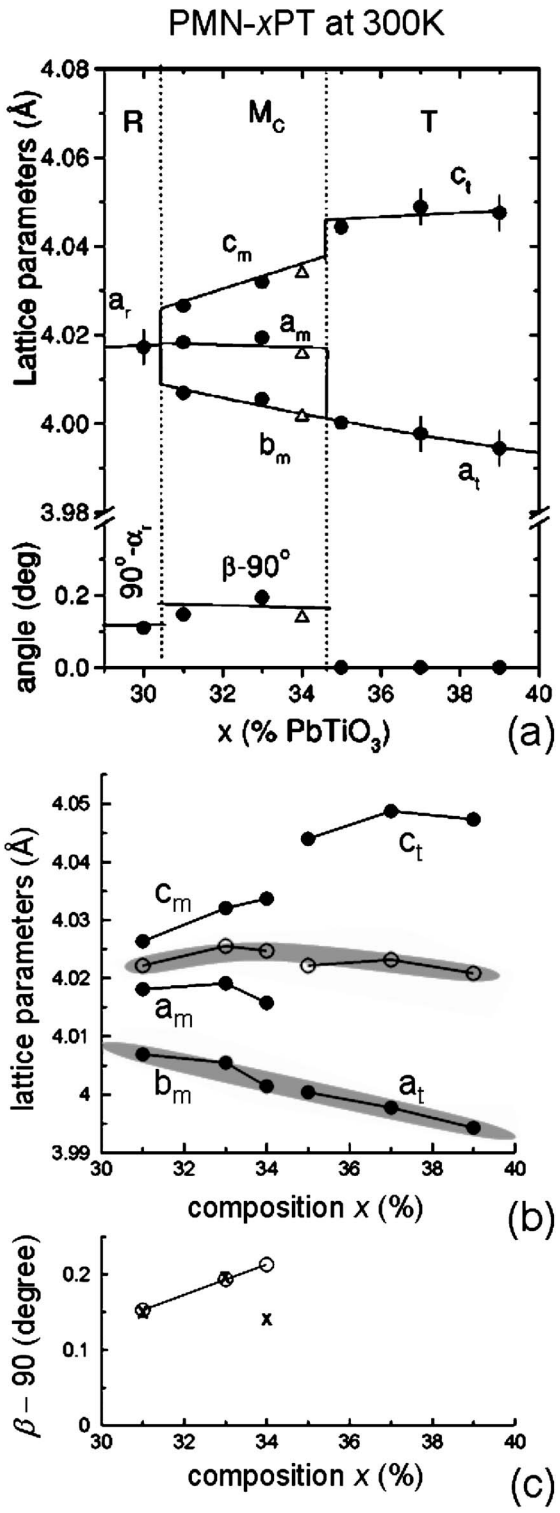

FIG. 5. Three intrinsic relationships of lattice parameters between the intermediate monoclinic M_C phase and conventional tetragonal phase of PMN-xPT at 300 K. (a) X-ray powder diffraction measurement of lattice parameters (reproduced with permission—Ref. 19), where the data for composition $x=34\%$ (open triangles) are taken from a different experiment. (b) The first and second intrinsic relationships are highlighted by gray shadow, where data are taken from (a). (c) The third intrinsic relationship is highlighted by line, where data of crosses (×) are taken from (a) and data of open circles (○) are calculated from Eq. (7c).

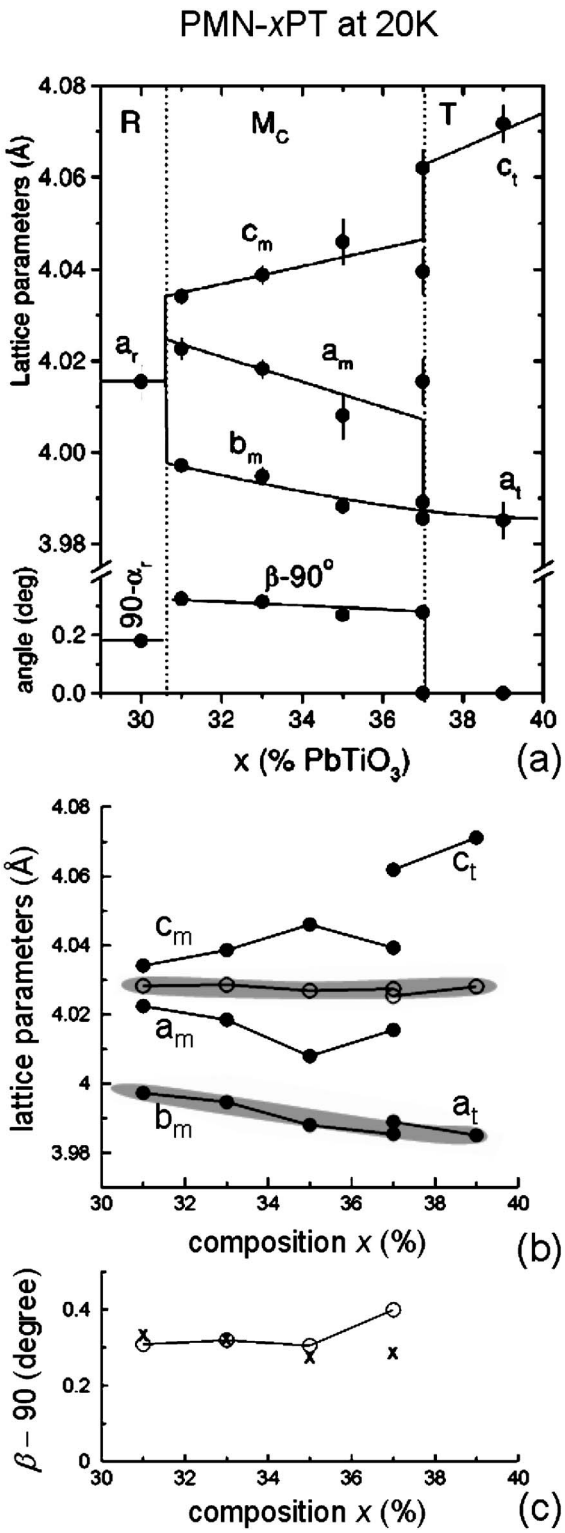

FIG. 6. Three intrinsic relationships of lattice parameters between the intermediate monoclinic M_C phase and conventional tetragonal phase of PMN-xPT at 20 K. (a) X-ray powder diffraction measurement of lattice parameters (reproduced with permission—Ref. 19). (b) The first and second intrinsic relationships are highlighted by gray shadow, where data are taken from (a). (c) The third intrinsic relationship is highlighted by line, where data of crosses (×) are taken from (a) and data of open circles (○) are calculated from Eq. (7c).

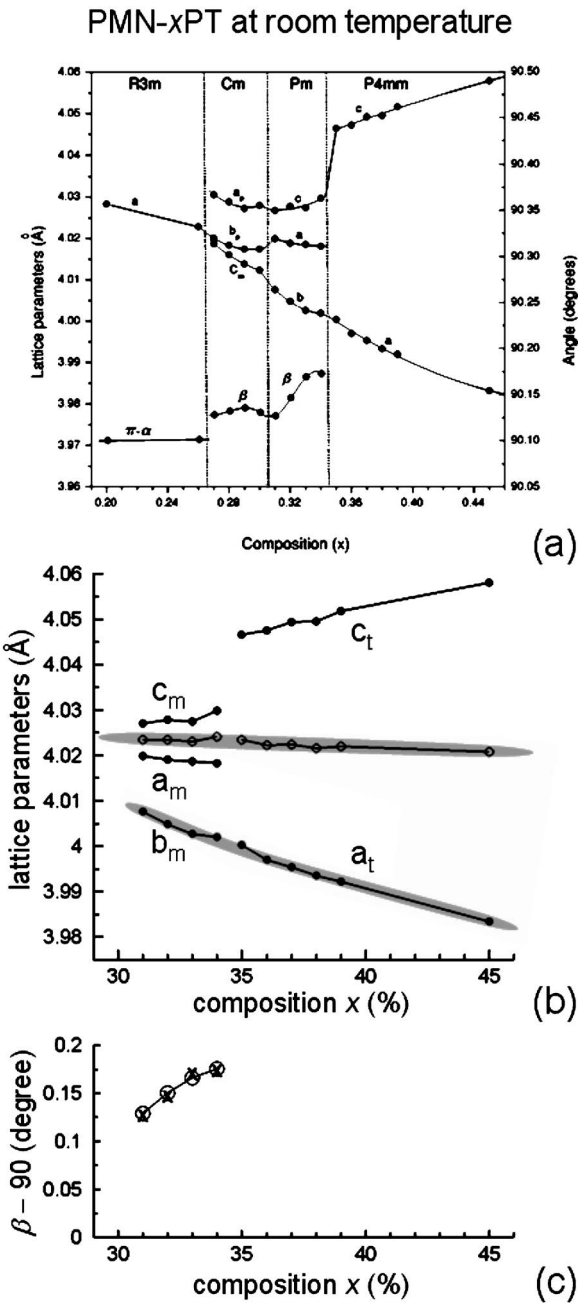

FIG. 7. Three intrinsic relationships of lattice parameters between the intermediate monoclinic M_C phase and conventional tetragonal phase of PMN-xPT at room temperature. (a) X-ray powder diffraction measurement of lattice parameters (reproduced with permission—Ref. 20). (b) The first and second intrinsic relationships are highlighted by gray shadow, where data are taken from (a). (c) The third intrinsic relationship is highlighted by line, where data of crosses (×) are taken from (a) and data of open circles (○) are calculated from Eq. (7c).

2. Temperature-dependent lattice parameters in zero-field cooling

a. PZN-10%PT. La-Orauttapong *et al.*[15] reported the temperature-dependent lattice parameters of PZN-10%PT in zero-field cooling by x-ray powder diffraction measurement as shown in Fig. 10(a). The three intrinsic relationships are shown in Figs. 10(b) and 10(c), with $A=0.71$. The volume fraction in the orthorhombic (monoclinic M_C) phase field is $\omega=\frac{1}{2}$. The monoclinic lattice parameters a_m, b_m, c_m, and β are calculated from the orthorhombic lattice parameters a_o, b_o, and c_o.

b. PZN-9%PT. Cox *et al.*[14] reported the temperature-dependent lattice parameters of PZN-9%PT in zero-field cooling by x-ray powder diffraction measurement as shown in Fig. 11(a). The three intrinsic relationships are shown in Figs. 11(b) and 11(c), with $A=0.72$. The volume fraction in the orthorhombic (monoclinic M_C) phase field is $\omega=\frac{1}{2}$. The monoclinic lattice parameters a_m, b_m, c_m, and β are calculated from the orthorhombic lattice parameters a_o, b_o, and c_o.

3. Temperature-dependent lattice parameters in field cooling

Ohwada *et al.*[10] reported the temperature-dependent lattice parameters of PZN-8%PT in field cooling with a [001] electric field of 2 kV/cm by single crystal neutron diffraction measurement as shown in Fig. 12(a). The first two intrinsic relationships are shown in Fig. 12(b). No monoclinic angle is reported to examine the third intrinsic relationship. Since only one data point in monoclinic M_C and tetragonal phases, respectively, is reported, the examination is only illustrative in this case.

4. Electric-field-dependent lattice parameters

Noheda *et al.*[9] reported the electric-field-dependent lattice parameters of PZN-8%PT in a [001] electric field by single crystal x-ray diffraction measurement as shown in Fig. 13(a). The three intrinsic relationships are shown in Figs. 13(b) and 13(c), with $A=0.76$. In the M_C phase field, the determined volume fraction ω is 0.529, 0.684, and 0.705 in increasing electric-field sequence. It is noted that the volume fraction ω of tetragonal variant 3 increases with increasing electric field, as expected from domain redistribution and domain-wall movement caused by an external electric field. Under increasing [001] electric field, the domain of a favorably oriented twin variant, i.e., variant 3 whose polarization $\mathbf{P}(3)$ is aligned with [001] axis, grows at the expense of the unfavorably oriented variant, leading to increase in ω. The averaged polarization $\mathbf{P}$ in Eq. (8) rotates in (010) symmetry plane during this process, as observed experimentally.

IV. DISCUSSIONS

Systematic analysis of extensive experimental data[9,10,14,15,19–21] presented in the preceding section confirms the theoretical prediction of three intrinsic relationships of lattice parameters between the recently discovered intermediate monoclinic M_C phase and the conventional ferroelectric tetragonal phase in PMN-xPT and PZN-xPT near the MPBs. These intrinsic relationships of lattice parameters are fulfilled by experimental data reported in the literature for different temperatures, compositions, and electric fields. They present quantitative evidence that the intermediate monoclinic M_C phase is a mixed state of nanometer-sized twin-related domains of the conventional ferroelectric tetragonal phase. The

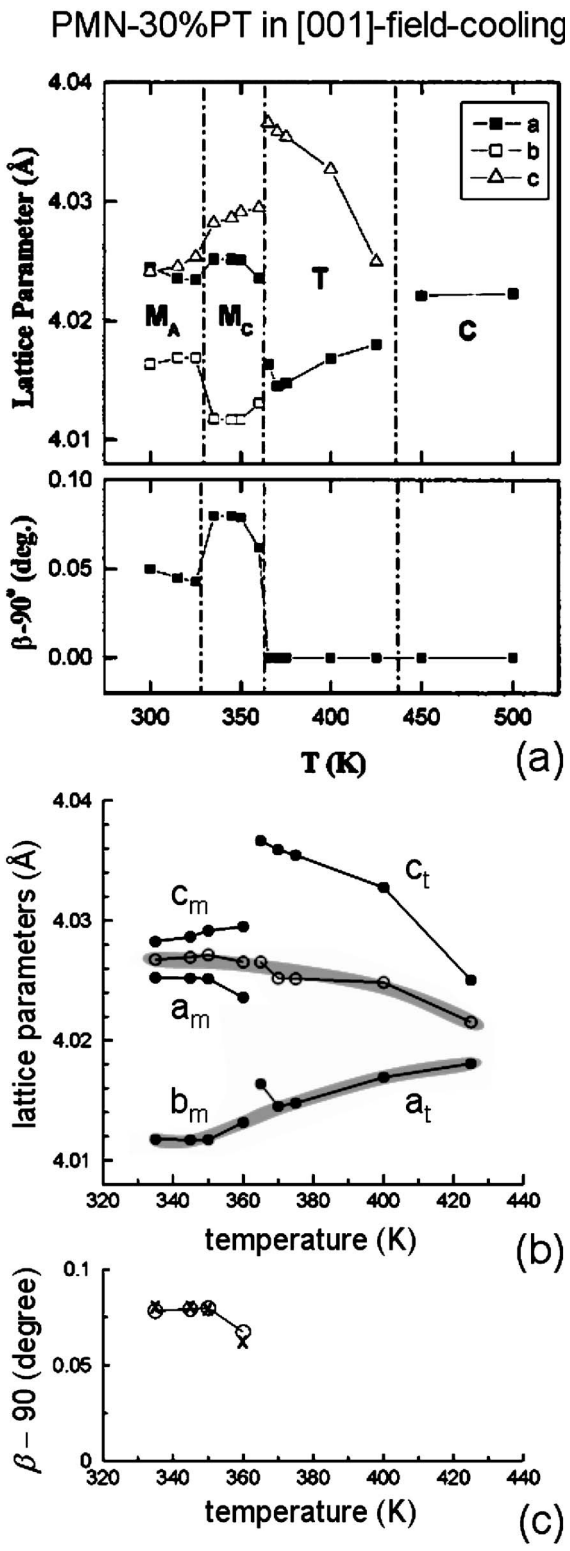

FIG. 8. Three intrinsic relationships of lattice parameters between the intermediate monoclinic M_C phase and conventional tetragonal phase of PMN-30%PT in field cooling with [001] electric field of 1 kV/cm. (a) Single crystal x-ray diffraction measurement of lattice parameters (reproduced with permission—Ref. 21). (b) The first and second intrinsic relationships are highlighted by gray shadow, where data are taken from (a). (c) The third intrinsic relationship is highlighted by line, where data of crosses (×) are taken from (a) and data of open circles (○) are calculated from Eq. (7c).

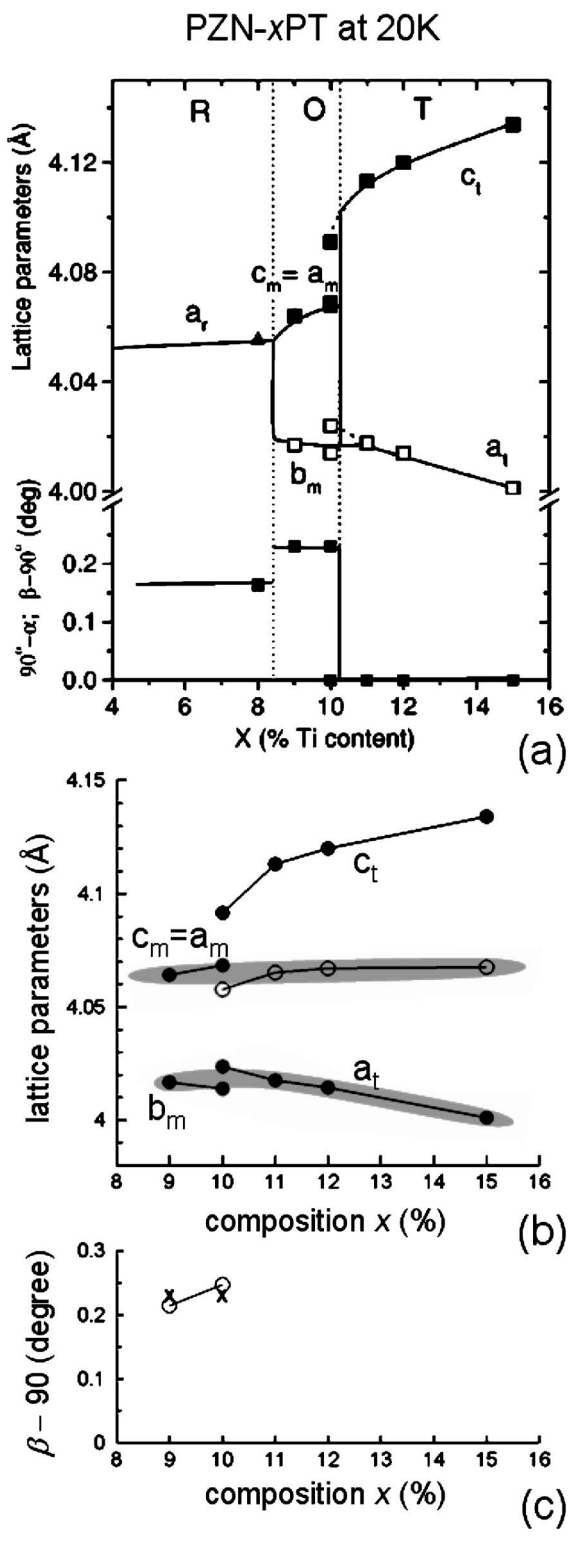

FIG. 9. Three intrinsic relationships of lattice parameters between the intermediate monoclinic M_C phase and conventional tetragonal phase of PZN-*x*PT at 20 K. (a) X-ray powder diffraction measurement of lattice parameters (reproduced with permission—Ref. 15). (b) The first and second intrinsic relationships are highlighted by gray shadow, where data are taken from (a). (c) The third intrinsic relationship is highlighted by line, where data of crosses (×) are taken from (a) and data of open circles (○) are calculated from Eq. (7c).

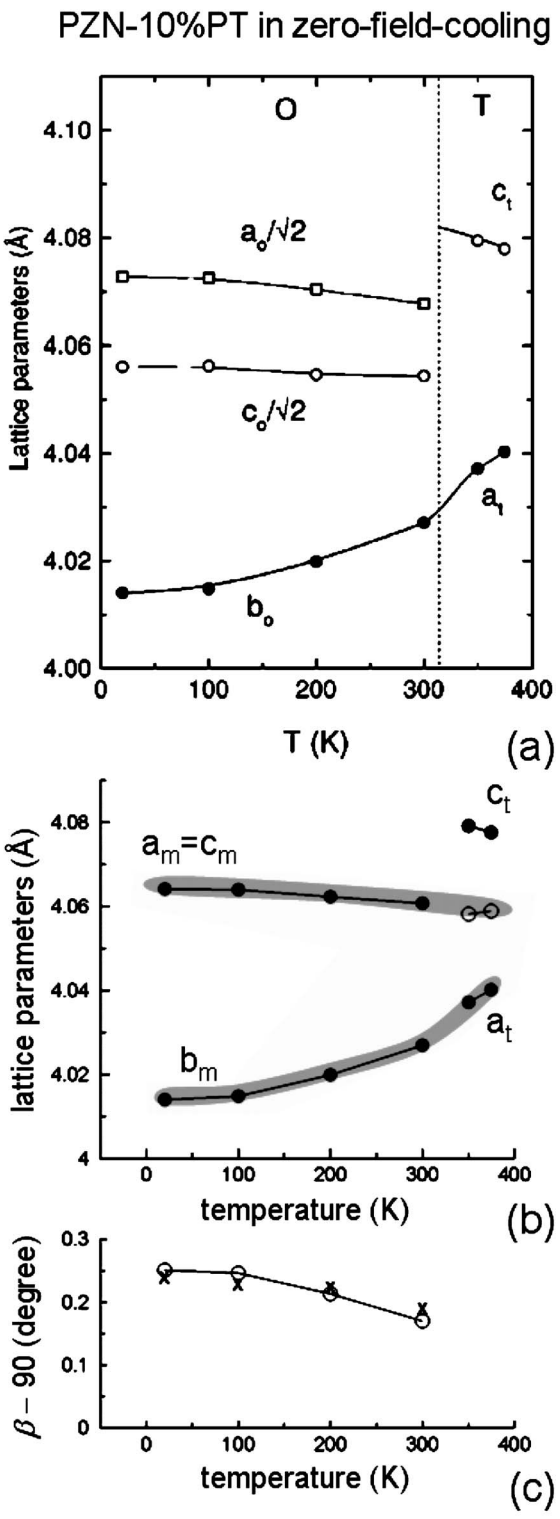

FIG. 10. Three intrinsic relationships of lattice parameters between the intermediate monoclinic M_C phase and conventional tetragonal phase of PZN-10%PT in zero-field cooling. (a) X-ray powder diffraction measurement of lattice parameters (reproduced with permission—Ref. 15). (b) The first and second intrinsic relationships are highlighted by gray shadow, where $a_m=c_m$ and b_m are calculated from (a). (c) The third intrinsic relationship is highlighted by line, where data of crosses (×) are calculated from (a) and data of open circles (○) are calculated from Eq. (7c).

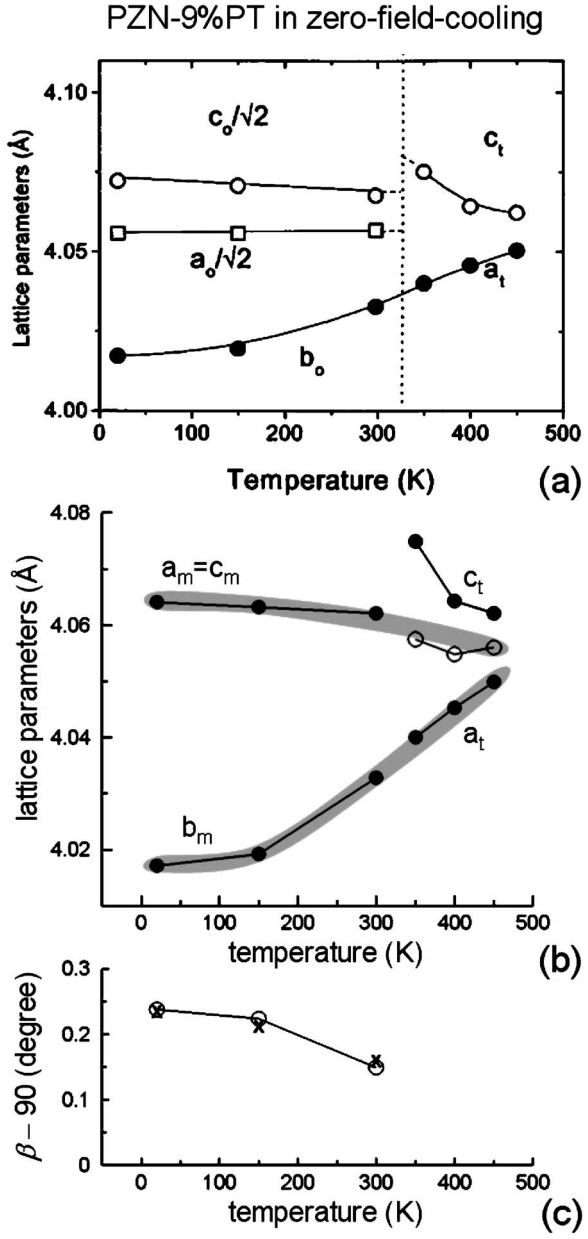

FIG. 11. Three intrinsic relationships of lattice parameters between the intermediate monoclinic M_C phase and conventional tetragonal phase of PZN-9%PT in zero-field cooling. (a) X-ray powder diffraction measurement of lattice parameters (reproduced with permission—Ref. 14). (b) The first and second intrinsic relationships are highlighted by gray shadow, where $a_m=c_m$ and b_m are calculated from (a). (c) The third intrinsic relationship is highlighted by line, where data of crosses (×) are calculated from (a) and data of open circles (○) are calculated from Eq. (7c).

analysis supports the viewpoint that the intermediate monoclinic M_C phase is an adaptive ferroelectric and ferroelastic phase,[29–31] which is homogeneous only on the macroscale while inhomogeneous on the nanoscale. Due to the small domain size and small ferroelastic strain, the conventional diffraction measurement does not resolve the lattice of individual nanodomains, but instead only perceives the average diffraction effect of nanotwins, which gives the experimentally observed monoclinic symmetry.

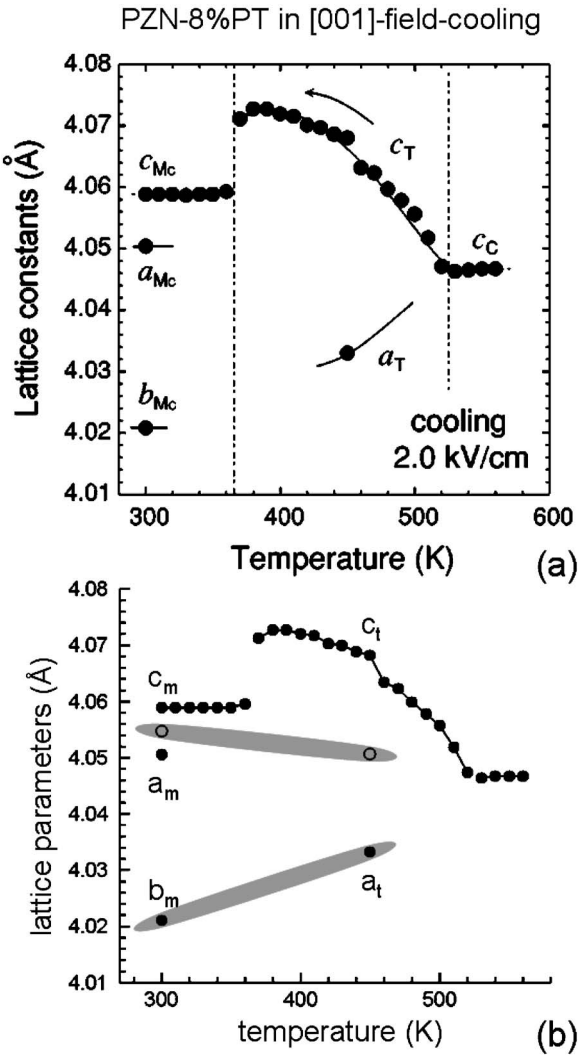

FIG. 12. Intrinsic relationships of lattice parameters between the intermediate monoclinic M_C phase and conventional tetragonal phase of PZN-8%PT in field cooling with [001] electric field of 2 kV/cm. (a) Single crystal neutron diffraction measurement of lattice parameters (reproduced with permission—Ref. 10). (b) The first and second intrinsic relationships are illustrated by gray shadow, where data are taken from (a).

It is worth noting that the second intrinsic relationship of lattice parameters, Eq. (7b), i.e., continuity between b_m and a_t, has been well recognized as a prominent feature in the reported experimental data[9,10,14,15,19–21] due to direct visual effect in data plots but without explanation. The concept of averaged nanotwins gives a natural explanation, as illustrated in Fig. 1. The two tetragonal twin variants have a common [010] axis with the same lattice parameter a_t, which is not affected by averaging and becomes the monoclinic lattice parameter b_m. It is noted that the nanotwins are structurally inhomogeneous, which gives broadening in diffraction profiles due to nanoscale domain size; however, the spacing of the {010} lattice planes, i.e., lattice parameter $b_m=a_t$, is homogeneous and is not affected by the nanotwin structure. Therefore, a sharp peak profile corresponding to (010) lattice spacing is expected to emerge in the diffraction pattern. Such

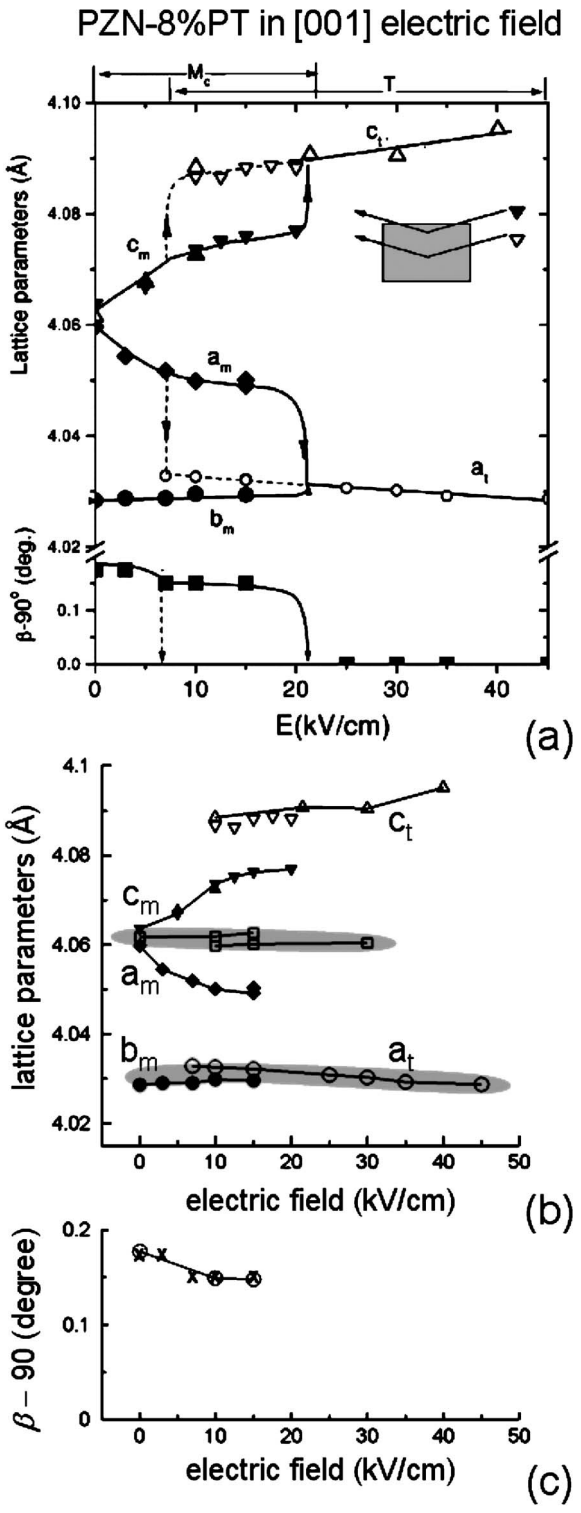

FIG. 13. Three intrinsic relationships of lattice parameters between the intermediate monoclinic M_C phase and conventional tetragonal phase of PZN-8%PT in [001] electric field. (a) Single crystal x-ray diffraction measurement of lattice parameters (reproduced with permission—Ref. 9). (b) The first and second intrinsic relationships are highlighted by gray shadow, where data are taken from (a). (c) The third intrinsic relationship is highlighted by line, where data of crosses (×) are taken from (a) and data of open circles (○) are calculated from Eq. (7c).

an anisotropic peak broadening phenomenon has been confirmed by x-ray diffraction experiments. Noheda *et al.*[19] found in x-ray powder diffraction of PMN-*x*PT that while broad features are associated with the diffraction profiles of low-temperature monoclinic M_C phase, the peak profile corresponding to the smallest lattice parameter b_m remains relatively sharp. Noheda *et al.*[9] also found unusual diffraction intensity distributions in single crystal x-ray diffraction of PZN-*x*PT for compositions close to the MPB, which are believed to reflect the existence of heavily twinned microstructures. Singh and Pandey[20] pointed out that the small ferroelastic strain and small domain size lead to the large broadening of the individual profiles and produce the signature of anomalous anisotropic peak broadening of some reflections. Ohwada *et al.*[10] believed that the asymmetry of Bragg-peak line shapes along the [001] or *c* axis indicates a nonuniform strain distribution within the crystal, which indeed is also an indication of inhomogeneous microstructure of nanotwins. All of these experimental observations are in agreement with the nanotwin viewpoint.[29–31]

The experimental data reported in the literature[9,10,14,15,19–21] are the lattice parameters of the majority phases only. Phase coexistence is normally observed near the MPBs. Singh and Pandey[20] reported the variation of molar fractions of the majority and minority phases with composition in PMN-*x*PT at room temperature obtained by Rietveld refinement of x-ray powder diffraction measurement, which shows that the monoclinic M_C and tetragonal phases coexist over a wide composition (x) range between 30% and 40%. Noheda *et al.*[19] reported the coexistence of the monoclinic M_C and tetragonal phases in PMN-33%PT over a wide temperature range, between 20 K and 300 K, with the volume fraction of the minority tetragonal phase found to be constant at about 25% over this entire temperature range. Figure 4(a) plots the temperature evolution of the monoclinic M_C and tetragonal lattice parameters of PMN-37%PT with an approximate volume fraction ratio 55:45 at both 20 K and 200 K.[19] The reported phase boundary is in fact a boundary between different majority phases. It is noted that the observed phase coexistence over such wide composition and temperature ranges cannot simply be explained by compositional fluctuation. However, according to the concept of the monoclinic M_C phase as a mixed state of nanotwins of the tetragonal phase, the structural phase transition between M_C and tetragonal phases is really a transition between small/nanodomain tetragonal phase and large-domain tetragonal phase. The large domains produce sharp and well-resolved peak profiles, which allow diffraction measurement to discern the tetragonal lattice of individual large domains.

Good agreement has been obtained between the theoretical prediction and the experimental data over the entire ranges of temperatures, compositions, and electric fields, as shown in Figs. 2–13. The three intrinsic relationships of lattice parameters are fulfilled within the accuracy of experimental measurement. The biggest discrepancy is found around the boundary between M_C and tetragonal phases. It is noted that the experimental data have the largest errors around this boundary. Because of the small domain sizes, diffraction peak broadening, and multiple coexisting phases, it is a difficult inverse problem to obtain lattice parameters from the complicated diffraction patterns. Nevertheless, our crystallographic analysis of the measured lattice parameters well reveals the three intrinsic relationships.

It is worth noting that the coefficient A in the third intrinsic relationship, Eq. (7c), is dependent on the domain size and the experimental measurement of the monoclinic angle by diffraction techniques (powder diffraction Rietveld refinement,[14,15,19,20] single crystal mesh scan).[9,21] As presented in Sec. III, the value of A is almost the same for PMN-*x*PT of different compositions and at different temperatures measured by x-ray powder diffraction at Brookhaven National Synchrotron Light Source,[19] i.e., $A=1.45$, 1.46, 1.51, and 1.45 for zero-field cooling of PMN-31%PT and PMN-33%PT, and PMN-*x*PT at 300 K and 20 K, respectively, except for zero-field cooling of PMN-37%PT where $A=1.04$. The data of PMN-*x*PT at room temperature measured by x-ray powder diffraction, performed at a different facility,[20] yields $A=1.20$. The data of PMN-30%PT in field cooling measured by mesh scan of single crystal x-ray diffraction, performed at Virginia Tech,[21] gives $A=0.74$. In the case of PZN-*x*PT, the value of A is almost the same for the data measured by x-ray powder or single crystal diffraction at Brookhaven National Synchrotron Light Source,[9,14,15] i.e., $A=0.64$, 0.71, 0.72, and 0.76 for PZN-*x*PT at 20 K, zero-field cooling of PZN-10%PT and PZN-9%PT, PZN-8%PT in an electric field, respectively. It is noteworthy that $A\approx 1.5$ for PMN-*x*PT in most cases, while $A\approx 0.7$ for PZN-*x*PT. As shown in Figs. 2–13 the third intrinsic relationship of the monoclinic angle is fulfilled by the experimental data. However, the dependence of the coefficient A on detailed diffraction experiment still requires further investigation. As our ongoing research, computational techniques are being employed to gain quantitative insight into this issue.

The three intrinsic relationships of lattice parameters present quantitative evidence of the tetragonal nanotwins. The result indicates that the electric-field-induced domain-wall movement is the origin of the ultrahigh electromechanical responses of these materials. The macroscopic strain of the sample associated with the conversion of ferroelastic variants is of the same order of magnitude as the spontaneous strain relating tetragonal twin variants. The largest electric-field-induced strain is obtained when the conversion of twin variants is complete. Using the reported tetragonal lattice parameters of PZN-8%PT in Fig. 13(a),[9] $c_t=4.087$ Å and $a_t=4.033$ Å in a [001] electric field of 10 kV/cm, the [001] elongation strain of twin variant conversion is $\varepsilon=(c_t-a_t)/a_t=1.3\%$. Viehland[13] has observed the electric-field-induced strain $\sim 1.2\%$ in [001]-oriented PZN-8%PT single crystal, which is in agreement with the theoretical prediction.

The existence of three intrinsic relationships of lattice parameters between the intermediate monoclinic M_C phase and the conventional ferroelectric tetragonal phase supports the viewpoint that the intermediate monoclinic M_C phase is adaptive phase.[29–31] Khachaturyan[31] shows that the monoclinic M_A phase is also an adaptive phase, which is a mixed state of nanotwins of the rhombohedral phase. Our analysis shows that the monoclinic M_B phase is also a mixed state (adaptive phase) of nanotwins of the rhombohedral phase, but with a distinct twin relationship from that of M_A phase.

In all cases of M_A, M_B, and M_C phases, the monoclinic symmetry is increased to orthorhombic symmetry at a particular twin volume fraction $\omega=\frac{1}{2}$, but corresponds to three different orthorhombic lattices O_A, O_B, and O_C, respectively. A transition between M_A or M_B and M_C (O_A and tetragonal or O_B and O_C in the limit case $\omega=\frac{1}{2}$) requires a rhombohedral-tetragonal phase transformation. It is noted that an electric-field-induced rhombohedral-to-tetragonal phase transformation has previously been proposed to explain the origin of ultrahigh electromechanical responses of PMN-xPT and PZN-xPT in Park and Shrout's pioneering work.[3] Also, in all cases, with the self-adjustment of nanodomain volume fraction ω in response to external electric field or applied stress, the averaged polarization continuously rotates in different symmetry planes, i.e., $(1\bar{1}0)$, $(\bar{1}01)$, or (010) in M_A, M_B, or M_C, respectively. A systematic analysis of the M_A and M_B phases will be reported elsewhere.

It has been pointed out that an explanation of the intermediate monoclinic phases in terms of the conventional Ginzburg–Landau–Devonshire theory of homogeneous ferroelectric phase is quite difficult.[29,30] The homogeneous ferroelectric monoclinic phase can be described only if eighth-order terms in the free energy expansion are introduced.[44] However, the theory cannot explain the observed three intrinsic relationships of lattice parameters reported here. From the perspective of self-assembling of nanodomains, the behaviors of the intermediate monoclinic phases have a conventional explanation: They are inherent features of a multidomain system quantitatively modified under the condition of low domain-wall energy density. Considering the energy degeneracy of polarization orientation among six tetragonal $\langle 001\rangle$ easy axes and eight rhombohedral $\langle 111\rangle$ easy axes near the MPBs, the electrocrystalline anisotropy would be greatly reduced. Recent first-principles calculations (based on an assumption of microscopic homogeneity of the ferroelectric order) have shown continuous polarization rotation as a low-free-energy path.[45] These calculations, in fact, demonstrate that the crystallographic anisotropy of the polarization direction is drastically reduced near the MPBs. Accordingly, the domain-wall energy density is also dramatically decreased, leading to domain miniaturization to nanoscale.

The results indicate that the electric-field-induced domain-wall movement plays an essential role in the ultrahigh electromechanical responses of PMN-xPT and PZN-xPT. It is noted that due to the small size of nanotwins, these materials contain high-density domain walls (twin boundaries). The high-density domain walls would produce peculiar material behaviors than that controlled by the bulk property of large domains. In particular, the property of domain walls will play a more significant role in determining the macroscopic property of the materials. The high-density domain walls will also make the materials more deformable than the large-domain materials because the domain walls are the carriers of the macroscopic strain induced by external electric field or applied stress. Therefore, it is worth further investigating the peculiar material behaviors dominated by high-density domain walls, which will help us better understand the origin of the ultrahigh electromechanical properties of these materials.

V. SUMMARY

Systematic analysis of extensive experimental data confirms the theoretical prediction of three intrinsic relationships of lattice parameters between the recently discovered intermediate monoclinic M_C phase and the conventional tetragonal phase in ferroelectric PMN-xPT and PZN-xPT near the MPBs. These intrinsic relationships of lattice parameters present quantitative evidence that the intermediate monoclinic M_C phase is a mixed state of nanotwins of the conventional ferroelectric tetragonal phase. The nanotwin microstructure explains the experimentally observed anisotropic broadening of diffraction peak profiles and phase coexistence over wide temperature and composition ranges. The results indicate that the electric-field-induced domain-wall movement plays an essential role in the ultrahigh electromechanical responses of these materials, and the high-density domain walls associated with the nanotwins produce peculiar material behaviors than that controlled by the bulk property of large domains, which is worth further investigation.

ACKNOWLEDGMENT

The financial support from Virginia Tech through startup fund is acknowledged.

*Electronic mail: yuwang@mse.vt.edu

[1] T. R. Shrout, Z. P. Chang, N. Kim, and S. Markgraf, Ferroelectr., Lett. Sect. **12**, 63 (1990).
[2] J. Kuwata, K. Uchino, and S. Nomura, Ferroelectrics **37**, 579 (1981).
[3] S. E. Park and T. R. Shrout, J. Appl. Phys. **82**, 1804 (1997).
[4] B. Jaffe, W. R. Cook, and H. Jaffe, *Piezoelectric Ceramics* (Academic, London, 1971).
[5] D. L. Polla and L. F. Francis, MRS Bull. **21**(7), 59 (1996).
[6] K. Uchino, *Ferroelectric Devices* (Marcel Dekker, New York, 2000).
[7] R. F. Service, Science **275**, 1878 (1997).
[8] B. Noheda, D. E. Cox, G. Shirane, S. E. Park, L. E. Cross, and Z. Zhong, Phys. Rev. Lett. **86**, 3891 (2001).
[9] B. Noheda, Z. Zhong, D. E. Cox, G. Shirane, S. E. Park, and P. Rehrig, Phys. Rev. B **65**, 224101 (2002).
[10] K. Ohwada, K. Hirota, P. W. Rehrig, Y. Fujii, and G. Shirane, Phys. Rev. B **67**, 094111 (2003).
[11] M. K. Durbin, J. C. Hicks, S. E. Park, and T. R. Shrout, J. Appl. Phys. **87**, 8159 (2000).
[12] J. M. Kiat, Y. Uesu, B. Dkhil, M. Matsuda, C. Malibert, and G. Calvarin, Phys. Rev. B **65**, 064106 (2002).
[13] D. Viehland, J. Appl. Phys. **88**, 4794 (2000).
[14] D. E. Cox, B. Noheda, G. Shirane, Y. Uesu, K. Fujishiro, and Y. Yamada, Appl. Phys. Lett. **79**, 400 (2001).
[15] D. La-Orauttapong, B. Noheda, Z. G. Ye, P. M. Gehring, J. Tou-

louse, D. E. Cox, and G. Shirane, Phys. Rev. B **65**, 144101 (2002).
[16] Y. Lu, D. Y. Jeong, Z. Y. Cheng, Q. M. Zhang, H. S. Luo, Z. W. Yin, and D. Viehland, Appl. Phys. Lett. **78**, 3109 (2001).
[17] D. Viehland and J. F. Li, J. Appl. Phys. **92**, 7690 (2002).
[18] A. K. Singh and D. Pandey, J. Phys.: Condens. Matter **13**, L931 (2001).
[19] B. Noheda, D. E. Cox, G. Shirane, J. Gao, and Z. G. Ye, Phys. Rev. B **66**, 054104 (2002).
[20] A. K. Singh and D. Pandey, Phys. Rev. B **67**, 064102 (2003).
[21] F. Bai, N. Wang, J. Li, D. Viehland, P. M. Gehring, G. Xu, and G. Shirane, J. Appl. Phys. **96**, 1620 (2004).
[22] Z. G. Ye, B. Noheda, M. Dong, D. Cox, and G. Shirane, Phys. Rev. B **64**, 184114 (2001).
[23] B. Noheda, D. E. Cox, G. Shirane, J. A. Gonzalo, L. E. Cross, and S. E. Park, Appl. Phys. Lett. **74**, 2059 (1999).
[24] B. Noheda, J. A. Gonzalo, L. E. Cross, R. Guo, S. E. Park, D. E. Cox, and G. Shirane, Phys. Rev. B **61**, 8687 (2000).
[25] A. G. Souza Filho, K. C. V. Lima, A. P. Ayala, I. Guedes, P. T. C. Freire, J. Mendes Filho, E. B. Araujo, and J. A. Eiras, Phys. Rev. B **61**, 14283 (2000).
[26] R. Guo, L. E. Cross, S. E. Park, B. Noheda, D. E. Cox, and G. Shirane, Phys. Rev. Lett. **84**, 5423 (2000).
[27] B. Noheda, D. E. Cox, G. Shirane, R. Guo, B. Jones, and L. E. Cross, Phys. Rev. B **63**, 014103 (2000).
[28] Ragini, R. Ranjan, S. K. Mishra, and D. Pandey, J. Appl. Phys. **92**, 3266 (2002).
[29] Y. M. Jin, Y. U. Wang, A. G. Khachaturyan, J. F. Li, and D. Viehland, Phys. Rev. Lett. **91**, 197601 (2003).
[30] Y. M. Jin, Y. U. Wang, A. G. Khachaturyan, J. F. Li, and D. Viehland, J. Appl. Phys. **94**, 3629 (2003).
[31] A. G. Khachaturyan (unpublished).
[32] M. E. Lines and A. M. Glass, *Principles and Applications of Ferroelectrics and Related Materials* (Clarendon, Oxford, 1977).
[33] A. G. Khachaturyan, *Theory of Structural Transformations in Solids* (Wiley, New York, 1983).
[34] E. K. H. Salje, *Phase Transitions in Ferroelastic and Co-elastic Crystals* (Cambridge University Press, Cambridge, UK, 1990).
[35] M. S. Wechsler, D. S. Lieberman, and T. A. Read, Trans. AIME **197**, 1503 (1953).
[36] J. S. Bowles and J. K. MacKenzie, Acta Metall. **2**, 129 (1954).
[37] A. G. Khachaturyan, Fiz. Tverd. Tela (S.-Peterburg) **8**, 2709 (1966); Sov. Phys. Solid State **8**, 2163 (1969).
[38] A. L. Roitburd, Fiz. Tverd. Tela (S.-Peterburg) **10**, 3619 (1968); Sov. Phys. Solid State **10**, 2870 (1969).
[39] A. G. Khachaturyan and G. A. Shatalov, Zh. Eksp. Teor. Fiz. **56**, 1032 (1969) [Sov. Phys. JETP **29**, 557 (1969)].
[40] A. L. Roytburd, Solid State Phys. **33**, 317 (1978).
[41] A. L. Roytburd, J. Phys. IV **5**, 21 (1995).
[42] A. G. Khachaturyan, S. M. Shapiro, and S. Semenovskaya, Phys. Rev. B **43**, 10832 (1991).
[43] S. M. Shapiro, B. X. Yang, G. Shirane, Y. Noda, and L. E. Tanner, Phys. Rev. Lett. **62**, 1298 (1989).
[44] D. Vanderbilt and M. H. Cohen, Phys. Rev. B **63**, 094108 (2001).
[45] H. Fu and R. E. Cohen, Nature (London) **403**, 281 (2000).